physica status solidi
www.pss-a.com

Conceptual Implementation of a Photonic–Plasmonic Transistor onto a Structured Nano-Guided Hybrid System

Giuseppe Emanuele Lio, Josslyn Beltran Madrigal, Christophe Couteau, Sylvain Blaize, and Roberto Caputo*

The interplay between quantum emitters and plasmonic nanostructures can unlock unprecedented functionalities, potentially useful for novel-concept photonics. Herein, the design and conceptual implementation of an integrated photonic–plasmonic transistor is reported. A mixed top-down and bottom-up nanofabrication approach is used to realize a prototype based on a nano-guided hybrid system enabling the interaction between gold nanostructures and emitters and thus resulting in a plasmon–exciton exchange. In analogy with a classical transistor (MOSFET), gold nanotapers (NTs) are fabricated in specific positions on a TiO_2 waveguide to behave as drain, source, and gate for highly localized electric near-fields. Photopolymerization by evanescent waves is then exploited to grow a polymeric ridge containing quantum dots directly on top of the NTs. The fluorescent spectroscopy of the prototype evidences a sensitive Purcell enhancement of the emission of the quantum dots located in proximity of the apices of gold NTs. The numerical study of the hybrid system demonstrates how this enhancement is controlled to efficiently route and modulate high-frequency optical signals in the novel photonic device.

1. Introduction

The continuous development of photonic and plasmonic solutions is increasingly influencing the downscaling of silicon-based devices to nanoscale features.[1–3] Classical transistors[4] have been thoroughly studied achieving many improvements also through their hybridization with organic materials,[5] by exploiting conduction properties of carbon nanotubes[6] or realizing them in very thin films of single-crystal oxide semiconductors.[7] The requirement of faster bitrates recently brought the attention to integrated photonics with first attempts considering bandgaps in dielectrics to realize power amplifiers[8] or photonic crystals in cross-waveguide geometry resulting in all-optical transistors.[9] The actual frontier in research is the implementation of photonic–plasmonic hybrids as transistors that exploit near-infrared[10,11] or (more rarely) visible radiation as a vector for signal transmission.[12] Such systems benefit from the confinement of high electric fields in small volumes typical of localized surface plasmons (LSPs) or surface plasmon polaritons (SPPs). First studies in this direction started with the realization of a PlasMOStor[13] including source, drain, and gate, as in case of a classical (MOSFET) transistor.[14] The state of the art of this kind of devices involves different aspects as ultrahigh bandwidth SPP-based information transfer,[15,16] and use of SPP optical nonlinearity for all-optical control.[17–19] Other aspects involve interactions related to strong and ultra-strong coupling of plasmon–photon systems[20–23] and coupling of single/multiple emitters with a waveguided mode.[24–27] Under the powerful thrust of these results, quantum plasmonics[28] is achieving a rapidly growing interest focussing on the study the quantum properties of light and its interaction with matter at the nanoscale. The realization of guided geometries, combining plasmonic and excitonic systems, then assumes a very intriguing character under both a fundamental and applicative point of view. Indeed, while nanoemitters have been mainly used in the past for improving the performance of photodiodes,[29] recent studies have successfully demonstrated relevant results like control of the spontaneous emission of light in the presence of metal nanostructures[30–34] and induced emission from quantum dots (QDs) by means of propagating LPSs.[35] Apart from their dramatic fundamental content, these studies suggest novel possibilities for integrated plasmonic–photonic applications. The sustainability of these systems for mass production has been demonstrated in both experimental[36,37] and theoretical studies.[38–40] In this communication, we propose the conceptual design of an integrated novel device where a nano-guided hybrid system promotes the interaction between gold nanostructures[41,42] and quantum emitters to enable a plasmon–exciton exchange procedure. For the design of the system, numerical calculations have determined the correct sizing of the involved components, whereas the fabrication of a

---

Dr. G. E. Lio, Prof. R. Caputo
Physics Department and CNR-Nanotec
University of Calabria
87036 Arcavacata di Rende (CS), Italy
E-mail: giuseppe.lio@unical.it

Dr. G. E. Lio, Dr. J. B. Madrigal, Prof. C. Couteau, Prof. S. Blaize
Laboratory Light, nanomaterials & nanotechnologies - L2n
University of Technology of Troyes & CNRS ERL7004
12 rue Marie Curie, 10300 Troyes, France

Prof. R. Caputo
Institute of Fundamental and Frontier Sciences
University of Electronic Science and Technology of China
Chengdu 610054, China

The ORCID identification number(s) for the author(s) of this article can be found under https://doi.org/10.1002/pssa.201900911.

DOI: 10.1002/pssa.201900911

proof-of-concept prototype is the result of combined top-down and bottom-up nanofabrication techniques.[43] A preliminary characterization of the realized system confirms the possibility to obtain an emission enhancement when the emitters are located in close proximity to plasmonic nanostructures.

2. Device Design

The goal of the proposed work is the conceptual design of a novel integrated device with functionalities as a photonic–plasmonic transistor (PPT). As shown in **Figure 1**, the PPT is composed by a glass substrate enclosing an ion exchange waveguide (IEW)[44] able to propagate a "bias" signal to the main arm of a T-shaped TiO_2 waveguide. A funnel-shaped side-arm couples a "modulation" signal into the guide through a diffraction grating. The TiO_2 guide collects both "bias" and "modulation" signals and evanescently couples them to the quantum emitters (QDs) and the metal nanostructures (triangular prism nanotapers [NTs]) situated above the guide in specific positions. The system works as a logic operator that modifies the optical supply like the classical one would do with the electrical supply. Through the main TiO_2 arm, the "bias" signal is absorbed by a first quantum emitter (donor, *D*) that reemits it (at a longer wavelength) nearby the apex of the first of two NTs located at controlled base-to-base distance (L_{bb}). These tapers are used to propagate the light emitted by *D* and thus behave as the optical "source" of the PPT. A second emitter (acceptor, *A*), positioned at the apex of the second taper, gathers the intense electric near-field in the hot-spot of the taper and reemits it to a third taper acting instead as the "drain" of the PPT. Finally, the signal coming from the side TiO_2 arm and passing through the taper orthogonal to the other ones is used to modulate the "bias" signal. For its specific role, the side taper behaves as the "gate" of the PPT and plays a fundamental role to achieve a typical MOSFET functionality.

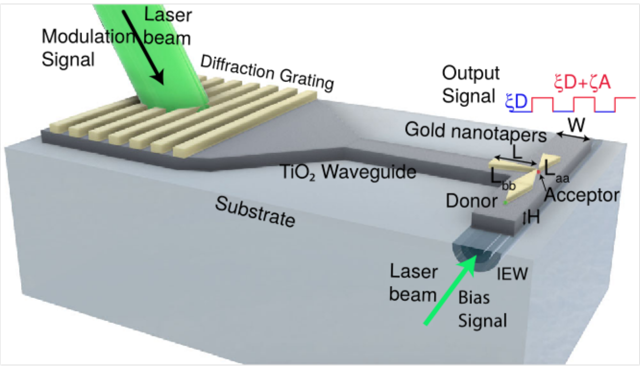

Figure 1. Sketch of the photonic–plasmonic transistor (PPT). A glass substrate encloses an ion exchange waveguide used to propagate a "bias" signal to the main arm of a T-shaped TiO_2 waveguide. A funnel-shaped side-arm couples a "modulation" signal into the guide through a diffraction grating. The TiO_2 guide collects both "bias" and "modulation" signals and evanescently couples them to the quantum emitters (QDs) and the metal nanostructures (triangular prism NTs), situated above the guide in specific positions. Through the main TiO_2 arm, the "bias" signal is absorbed by a first quantum emitter (donor, *D*) that reemits it (at a longer wavelength) nearby the apex of the first of two NTs, located at controlled base-to-base distance. These NTs propagate the light emitted by *D*, thus behaving as the optical "source" of the PPT. A second emitter (acceptor, *A*), positioned at the apex of the second taper, gathers the intense electric near-field in the hot-spot of the taper and reemits it to a third taper acting instead as the "drain" of the PPT. Finally, the signal coming from the side TiO_2 arm and passing through the taper orthogonal to the other ones is used to modulate the "bias" signal. For its specific role, the side taper performs the function of the "gate" of the PPT and plays a fundamental role to achieve a typical MOSFET functionality.

2.1. Design of the Photonic–Plasmonic Transistor

The first aim of the theoretical study is the correct sizing of the TiO_2 waveguide to select a single mode propagation.[45–47] Finite element method (FEM) simulations have been performed to obtain optimal values for thickness (*H*) and width (*W*) of the dielectric waveguide. The presence of a single mode is assured by $H = 150$ nm and $W = 500$ nm, convenient enough values for the nanofabrication. Regarding the polarization of the confined light, past studies demonstrate that the best propagation is observed in case of transversal magnetic polarization. In the same study, the simulation is reported for choosing the features of the single NT (thickness = 50 nm, width = 250 nm, and length = 750 nm)[48] (insets in **Figure 2**b). Following this preliminary design step, the overall functioning of the prototype is considered. For this reason, the donor, simulated by an oscillating dipole and placed on top of the TiO_2 waveguide, emits the "bias" signal passing through the "source" (base-to-base) NTs. By normalizing the power of the signal transmitted by the first NT (Figure 2a, white dashed line) with the power emitted by the donor, it is possible to calculate the efficiency of the device. According to the numerical simulations, the efficiency is evaluated as the ratio between the absorbed power and the total power sent through the NTs.

The efficiency of the device is optimized by varying the base-to-base (L_{bb}) and apex-to-apex (L_{aa}) NTs gaps (Figure 2a). Numerical simulations demonstrate that the best efficiency value (close to 60%, Figure 2b) is obtained when both gaps are zero, as in a typical bowtie configuration.[49,50] In the real experiment, it has been chosen $L_{bb} = 0$ nm and $L_{aa} = 50$ nm. The choice for L_{aa} results in a twofold advantage. First, this value is close to the lowest limit for lithography; second, the apex-to-apex gap represents a useful host site for the acceptor (*A*). On the contrary, the interaction between nanoemitters and SPPs depends on the distance from the emitter to the plasmonic structures. Barnes et al.[51] show the results for the coupling between a dipole and SPPs. The plots reported in ref. [48] show the fraction of power dissipated into different decay channels related to the orientation of a dipole and the dipole–metal distance. For small distances (generally shorter than 40 nm), the dipole is mainly coupled to lossy waves. At this scale, the transfer of energy from the dipole to the metal nanostructures can generate an electron–hole pair and this energy can be dissipated by the metal. Noteworthy, even with $L_{aa} = 50$ nm, the efficiency results in a 40% value. In the numerical simulations, an estimated input (optical) power of 1 mW is used as "bias" signal. This input power is enough to excite the first QD (the donor, *D*), and then the signal travels through the whole system until it reaches the acceptor *A*.

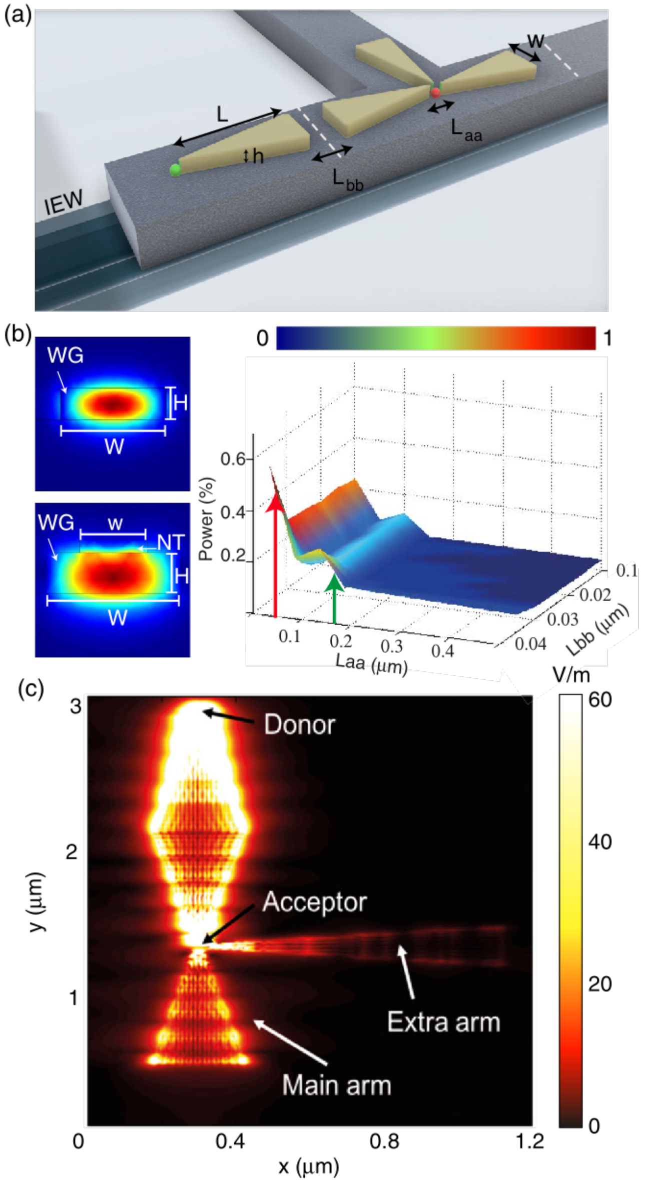

Figure 2. Sketch of the geometry used to simulate exciton–plasmon exchange processes as a function of size and relative distances between NTs. a) On the main arm are situated three NTs; in the simulation the signal goes through the first two NTs and it is collected in the absorption "box," where the acceptor should be positioned; b) the graph shows the efficiency when the distances L_{aa} and L_{bb} between the NTs change. The two insets depict the single mode propagation inside the TiO_2 waveguide (top), and with the gold NTs placed on top of it (bottom); c) the electric field map shows the light propagation from "source" to "drain." The numerical simulation is performed by considering a single emitter in the position of the donor and studies how both emitted light and SPPs propagate through the system arriving in each considered position: acceptor site, apex of the "gate" NT, and "drain."

For modulating the "bias," another signal (also 1 mW power) is sent from the extra-arm. About the estimation of the efficiency of the device, this is in the "upper" state when the sum of "bias" and "modulation" signals overcomes the 40% of 2 mW (0.80 mW). The device is in the "lower" state in the opposite case (under 40% of 2 mW). Simulations also highlight the interplay between deterministic sources and plasmonic nanostructures,[52,53] and reveal the physical mechanisms responsible of the whole PPT device functioning. As shown in Figure 2c, by evanescently exciting the donor with light coming from the TiO_2 waveguide, an exciton–plasmon transfer mechanism takes place that allows the signal propagation from D to A, through the (base-to-base) NTs. The figure shows the field map of the whole device under an ideal emission from the nanoemitter (D) involved in the system at the apex of the "source." In fact, the evanescent wave propagates along the NTs edge arriving in each considered position as the acceptor site (A), the apex of the "gate" and the "drain" output site. At this point, the "bias" signal, absorbed and reemitted by A, is collected by the apex of the following "drain" NT. By considering the several energy exchange processes involved, we can suppose that only a fraction ξD of the original "bias" signal arrives to the drain. In a typical transistor analogy, the modulation of the "bias" signal is achieved by pumping the QD A through the "gate" NT (side-arm waveguide). As already anticipated, the "modulation" signal is dispatched to this NT when the corresponding waveguide is illuminated through the diffractive coupler. The sketch in Figure 1 shows a modulated signal at the end of the "drain" base where the lower state "0" is only represented by ξD, whereas the upper state "1" is given by the sum $\xi D + \zeta A$. This can be obtained by switching "on" and "off" the light pumping on the "gate" that results in a control of the optical signal between upper and lower states at very high rates. The best coupling efficiency between nanoemitters and plasmonic structures is numerically studied by varying the size of each considered element, thus finding the best value. In doing so, we have used the overlap integral that represents the energy transfer from a mode 1 to a mode 2, as reported in the following equation:

$$\eta = \frac{1}{P_0}\mathrm{Re}\left(\frac{\int_A E_1 \times H_2 * \cdot \hat{z}\mathrm{d}A \cdot \int_A E_2 \times H_1 * \cdot \hat{z}\mathrm{d}A}{\int_A E_1 \times H_1 * \cdot \hat{z}\mathrm{d}A}\right) \tag{1}$$

where η is the correlation coefficient, E_1 and H_1 correspond to the electromagnetic field of the mode 1 and E_2 and H_2 for the mode 2, A is the area of the mode, and P_0 is the mode power. Finally, the spontaneous emission (SE) rate has been derived from the Purcell factor (PF) for nanostructured cavities.[54] The SE evaluation plays a fundamental role in this kind of device; in fact, it establishes the limit that inhibits the emission. Here, the considered equation is

$$\gamma_{\mathrm{SE}}^{\mathrm{Max}} = \frac{\sqrt{6\omega\gamma_0}}{\pi} \tag{2}$$

that ensures the maximum of the spontaneous emission from the nanoemitters placed in the nanocavity (the cross of the NTs). Here, $\gamma_0 = 1/\tau$ and τ are typically of the order of 100×10^{-12}s.

2.2. Fabrication of the Photonic–Plasmonic Transistor

The realization of the prototype is the result of a mixed top-down and bottom-up approach performed in an addictive

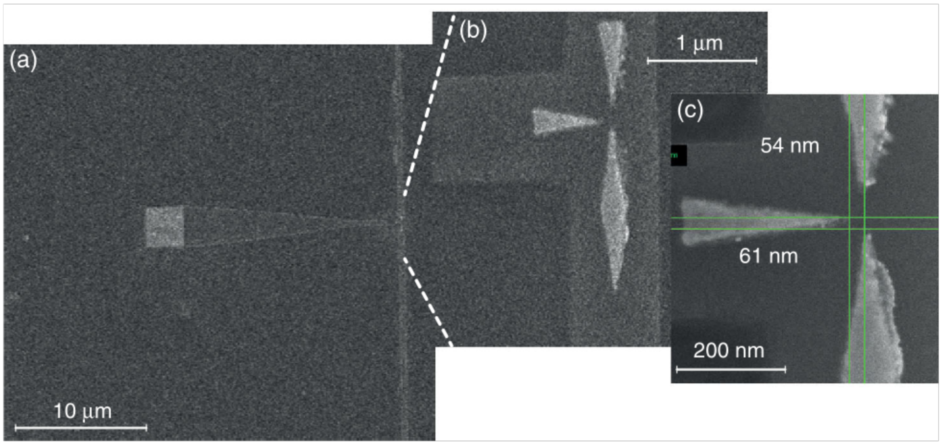

Figure 3. Picture of the actual prototype realized by EBL and PVD. a) By observing the whole system from the top, it is possible to distinguish the TiO_2 waveguide realized above the IEW, the gold diffractive coupler, and the NTs; b) a zoom-in of the core of the device; and c) detail of the distances between the side NT and the apex-to-apex NTs.

manufacturing scheme. A first top-down procedure, electron beam lithography (EBL) and physical vapor deposition (PVD), is devoted to the nanofabrication of the T-shaped TiO_2 waveguide (150 nm thickness) (**Figure 3**a). The substrate of the prototype is a glass slab comprising an ion-exchange waveguide covered by the main arm of the TiO_2 waveguide. Following the TiO_2 waveguide fabrication, a top-down fabrication step (EBL) realizes the gold NTs ("source," "drain," and "gate" of the PPT) and the gold grating exploited as in-coupler for the "modulation" signal. After the EBL procedure, PVD is utilized in two consequent phases: the deposition of an SiO_2 adhesion layer (30 nm thickness) and an gold layer (50 nm thickness) (Figure 3b,c). After a final lift-off step, most part of the fabrication of the integrated device is done except for the positioning of the quantum emitters. This phase requires particular attention because the emitters need to be located in close proximity of the NTs apices.

Indeed, this is the most delicate part of the fabrication procedure because these (ideally) single emitters are responsible of the exciton–plasmon exchange fundamental for the device functioning. An effective bottom-up approach to challenge this difficulty is to adopt a process of nanophotopolymerization by evanescent waves (PEW).[55,56] In detail, a very thin layer of a photoresin grafted with QDs (CdSe) is cured directly on top of the main arm of the TiO_2 waveguide. In this process, the light channeled into the IEW couples with the TiO_2 waveguide and generates evanescent waves at the interface between TiO_2 and the photoresin layer. The curing of the QDs-doped photoresin, due to highly localized near-fields of the evanescent waves, precisely carves a polymeric ridge of few nanometers thickness in the liquid photoresin. The photoresin utilized in the experiment is a mixture of polymer PETA (pentaerythritol triacrylate) + 4 wt% of MDEA (methyl diethanolamine) + 0.5 wt% of Eosin Y + 1 wt% of CdSe nanocrystals. It absorbs visible light in a range from 400 to 540 nm, with a peak at 530 nm, and emits light at 590 nm. The technique allows realizing polymer ridges containing nanoemitters with a restrained thickness as low as 18 ± 2 nm.[57]

3. Characterization and Discussion

The ideal design of the PPT predicts the presence of deterministic sources in proximity of the NTs apices, performing as donor and acceptor (Figure 1) of the "bias" light signal. The result of the PEW nanofabrication experiments is a polymer ridge containing QDs and covering the whole main arm of the device. This result is actually the first step toward the realization of a working PPT. However, it represents a valuable workbench to study the modification of the plasmon–exciton interaction in different positions along the ridge. Indeed, a sensitive enhancement of the output fluorescence emission intensity is expected in those points of the ridge where deterministic sources are located in close proximity to plasmonic tapers. In that case, the huge amount of light localized to extremely small volumes by the plasmonic nanostructures is strongly absorbed by the QDs. A better physical insight of this phenomenon is provided by the PF of the system or how the emission properties of quantum sources are modified by their surrounding environment. As shown in previous studies, the PF of a single quantum emitter is written as[58]

$$\mathrm{PF} = \frac{P}{P_0} = \frac{E/C}{E_0/C} = \frac{E}{E_0} = \frac{\hbar\lambda}{\hbar\lambda_0} = 1.47 \tag{3}$$

where P is the power emitted by the dipole source (590 nm) and P_0 is instead the laser power used to excite the system (400 nm). In our case, we expect a somehow higher value because the photopolymerized ridge contains several QDs combined with the Eosin Y dye material that together produce a multiexciton emission.[59] Moreover, the particular geometry designed for the PPT includes NTs, as plasmonic enhancers, that can strongly influence the output signal intensity.[60,61] To verify the validity of this description, fluorescent spectroscopy experiments have been performed on the fabricated sample. In particular, emission spectra have been acquired in three different points (**Figure 4**a): exactly in correspondence of the NTs (blue circle), on the bare TiO_2 waveguide (green circle), and finally on the IEW (red circle). In the experiment, a blue laser ($\lambda = 405$ nm) is used to excite the

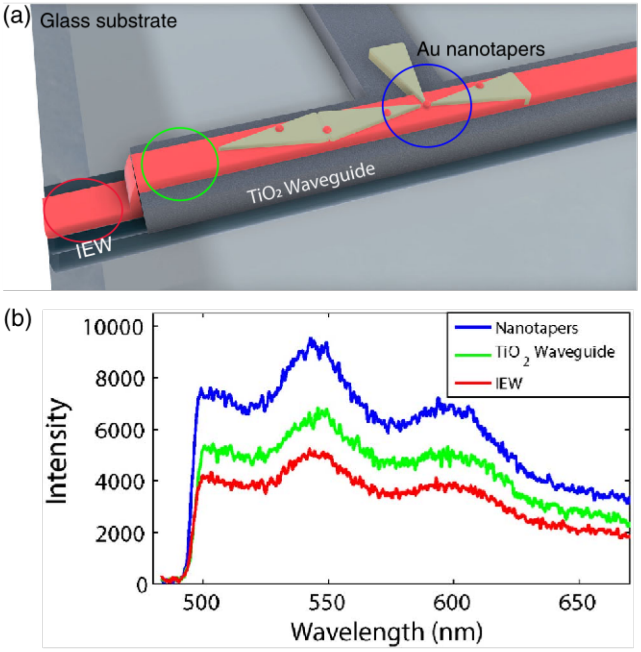

Figure 4. Fluorescent spectroscopy experiments performed on the realized device. a) The QDs-doped ridge, fabricated by nanophotopolymerization by evanescent waves onto the main arm of the TiO_2 waveguide, is depicted as a red layer. The three circles of different color represent the areas analyzed by confocal microscope to collect the emission from nanoemitters; b) the graph shows the emission in three different cases: close to NTs (blue line); exactly on the TiO_2 waveguide (green line); and on the IEW (red line). The two mains peaks in the graph correspond to the Eosin Y emission at 545 nm and the CdSe QDs emission at 590 nm.

QDs, and the emission signal is collected by a confocal microscope equipped with a fluorescent spectrometer. Figure 4b shows the comparison of the spectra acquired in different points of the sample. The emission intensity undergoes a considerable increase when the signal is acquired in proximity of the gold nanostructures with a value that is double of the one measured on the bare IEW.

The obtained result represents the first possibility to implement a multiband photonic structure using waveguides, plasmonic gold nanostructures, and nanoemitters. Several numerical simulations have been performed (Fullwave FDTD by RSoft) to demonstrate the performance of the realized prototype in terms of output power and modulation frequency. In the simulations, the geometric parameters of the realized prototype have been utilized ($L_{aa} = 150\,\text{nm}$ and $L_{bb} = 0\,\text{nm}$) that, according to the surface of Figure 2b, provide an overall output power efficiency of about 10%. In a first simulation, a single dipole source is used to model the donor (D) emitting the "bias" signal that propagates through the NTs and is finally collected as an output signal at the drain taper. As explained earlier, the output signal is only a fraction ξD of the original bias signal (1 mW) that is attenuated by energy exchange processes and intrinsic plasmonic losses of the tapers (blue line in **Figure 5**). The second simulation involves two dipole sources, respectively, located in the position of the donor (D) and the acceptor (A). In this case, the output signal is the combination of donor (ξD) and acceptor (ζA) contributions (red line in Figure 5). The third simulation takes into account the donor as always on and a modulating behavior for the acceptor with on–off periodic intervals of about 10 ns. The result of this simulation is the dashed green line in Figure 5. Due to the on–off switching of the gate signal (acceptor), the (green) line is modulated by very short rise and fall times (few ns) that reflect the possibility to control the optical signal at very high-frequency rates. For what concerns the output power, the modulation increases the output power from the 2% to the 10% that, considering an initial equal power of 1 mW for both donor and acceptor, corresponds to estimated $\xi = 0.2$ and $\zeta = 0.8$.

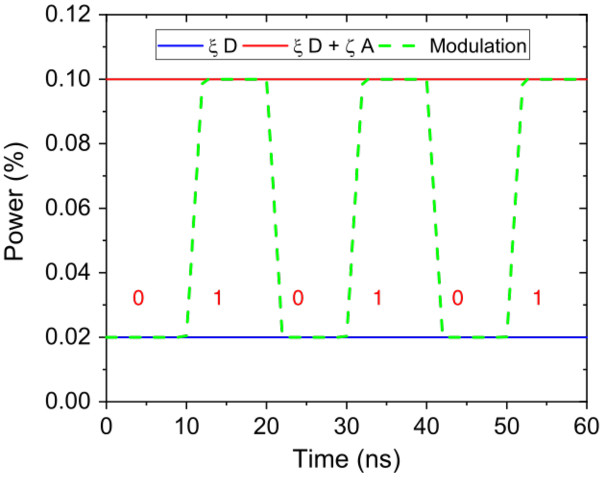

Figure 5. The modulation of the output power according to the numerical simulations. The blue line shows the output signal (ξD) when the donor only is on; the red line displays the sum output $\xi D + \zeta A$ when both donor and acceptor are on; the dashed green line is the output modulation when the acceptor is periodically switched on and off. The modulation increases the output power from the 2% to10%.

4. Conclusions

In this work it has been presented the conceptual realization of a hybrid device exploiting principles of photonics, plasmonics, nanoelectronics, and nanooptoelectronics. After the design of the device, an additive manufacturing procedure including standard nanofabrication (e-beam lithography) and nanoemitters positioning by evanescent wave photo-polymerization was necessary for its realization. QDs have been dispersed in a tiny polymeric ridge extending along the whole device area. This is not yet the aimed result though represents a helpful workbench to test the Purcell emission enhancement of QDs located in proximity of plasmonic nanostructures. To theoretically verify the functionalities of the device in analogy to a classical transistor, FDTD numerical simulations have been performed whose results demonstrate the high-frequency modulation of the optical signal output from the device. Overall, the conceptual study provides a useful insight on the design and production of an integrated circuit able to work in the visible range.

Acknowledgements

The authors thank Stefano Pierini and Renaud Bachelot for fruitful discussions. The authors would like to acknowledge the contribution of the COST Action CA16220 and the EUIMWP COST Ph.D. and ECI meeting hosted in Ljubljana. The authors thank the UTT (University of Technology of Troyes) for the opportunity to study and realize the structures presented in this work, and the GrandEst regional platform "Nanomat" for nanofabrication and nanocharacterisation. The authors also thank the "Area della Ricerca di Roma 2," Tor Vergata, for the access to the ICT Services (ARToV-CNR). This article was amended on June 5, 2020 to correct the title of the manuscript and figure 1.

Conflict of Interest

The authors declare no conflict of interest.

Keywords

photonics, plasmonics, quantum emitters, transistors

Received: November 4, 2019
Revised: April 22, 2020
Published online: May 5, 2020

[1] R. Soref, *IEEE J. Sel. Top. Quant. Electron.* **2006**, *12*, 1678.
[2] E. Ozbay, *Science* **2006**, *311*, 189.
[3] D. E. Chang, A. S. Sørensen, E. A. Demler, M. D. Lukin, *Nat. Phys.* **2007**, *3*, 807.
[4] R. P. Jain, *Modern Digital Electronics*, Tata McGraw-Hill Education, New Delhi **2003**.
[5] R. Tecklenburg, G. Paasch, S. Scheinert, *Adv. Funct. Mater.* **1998**, *8*, 285.
[6] A. D. Franklin, M. Luisier, S.-J. Han, G. Tulevski, C. M. Breslin, L. Gignac, M. S. Lundstrom, W. Haensch, *Nano Lett.* **2012**, *12*, 758.
[7] K. Nomura, H. Ohta, K. Ueda, T. Kamiya, M. Hirano, H. Hosono, *Science* **2003**, *300*, 1269.
[8] V. Radisic, Y. Qian, T. Itoh, *IEEE Microwave Guided Wave Lett.* **1998**, *8*, 13.
[9] M. F. Yanik, S. Fan, M. Soljačić, J. D. Joannopoulos, *Opt. Lett.* **2003**, *28*, 2506.
[10] T. Rauch, M. Böberl, S. F. Tedde, J. Fürst, M. V. Kovalenko, G. Hesser, U. Lemmer, W. Heiss, O. Hayden, *Nat. Photonics* **2009**, *3*, 332.
[11] M. Abb, Y. Wang, N. Papasimakis, C. De Groot, O. L. Muskens, *Nano Lett.* **2014**, *14*, 346.
[12] J. Tominaga, C. Mihalcea, D. Büchel, H. Fukuda, T. Nakano, N. Atoda, H. Fuji, T. Kikukawa, *Appl. Phys. Lett.* **2001**, *78*, 2417.
[13] J. A. Dionne, K. Diest, L. A. Sweatlock, H. A. Atwater, *Nano Lett.* **2009**, *9*, 897.
[14] E. H. Nicollian, J. R. Brews, E. H. Nicollian, *MOS (Metal Oxide Semiconductor) Physics and Technology*, Vol. *1987*, Wiley, New York **1982**.
[15] P. N. Melentiev, A. Kalmykov, A. Kuzin, D. Negrov, V. Klimov, V. I. Balykin, *ACS Photonics* **2019**, *6*, 1425.
[16] J. Chen, Z. Li, S. Yue, Q. Gong, *Nano Lett.* **2011**, *11*, 2933.
[17] W. Dickson, G. A. Wurtz, P. R. Evans, R. J. Pollard, A. V. Zayats, *Nano Lett.* **2008**, *8*, 281.
[18] Y. Fu, X. Hu, C. Lu, S. Yue, H. Yang, Q. Gong, *Nano Lett.* **2012**, *12*, 5784.
[19] D. Pacifici, H. J. Lezec, H. A. Atwater, *Nat. Photonics* **2007**, *1*, 402.
[20] B. Munkhbat, M. Wersäll, D. G. Baranov, T. J. Antosiewicz, T. Shegai, *Sci. Adv.* **2018**, *4*, eaas9552.
[21] Y. Fedutik, V. Temnov, O. Schöps, U. Woggon, M. Artemyev, *Phys. Rev. Lett.* **2007**, *99*, 136802.
[22] V. Muravev, I. Andreev, I. Kukushkin, S. Schmult, W. Dietsche, *Phys. Rev. B* **2011**, *83*, 075309.
[23] A. F. Kockum, A. Miranowicz, S. De Liberato, S. Savasta, F. Nori, *Nat. Rev. Phys.* **2019**, *1*, 19.
[24] M. J. Morrissey, K. Deasy, Y. Wu, S. Chakrabarti, S. Nic Chormaic, *Rev. Sci. Instrum.* **2009**, *80*, 053102.
[25] K. Nayak, P. Melentiev, M. Morinaga, F. Le Kien, V. Balykin, K. Hakuta, *Opt. Express* **2007**, *15*, 5431.
[26] M. Fujiwara, K. Toubaru, T. Noda, H.-Q. Zhao, S. Takeuchi, *Nano Lett.* **2011**, *11*, 4362.
[27] M. Gaio, M. Moffa, M. Castro-Lopez, D. Pisignano, A. Camposeo, R. Sapienza, *ACS Nano* **2016**, *10*, 6125.
[28] M. S. Tame, K. McEnery, Ş. Özdemir, J. Lee, S. A. Maier, M. Kim, *Nat. Phys.* **2013**, *9*, 329.
[29] A. J. Shields, M. O'sullivan, I. Farrer, D. Ritchie, R. Hogg, M. Leadbeater, C. Norman, M. Pepper, *Appl. Phys. Lett.* **2000**, *76*, 3673.
[30] A. O. Govorov, G. W. Bryant, W. Zhang, T. Skeini, J. Lee, N. A. Kotov, J. M. Slocik, R. R. Naik, *Nano Lett.* **2006**, *6*, 984.
[31] A. De Luca, M. Ferrie, S. Ravaine, M. La Deda, M. Infusino, A. R. Rashed, A. Veltri, A. Aradian, N. Scaramuzza, G. Strangi, *J. Mater. Chem.* **2012**, *22*, 8846.
[32] M. Infusino, A. De Luca, A. Veltri, C. Vázquez-Vázquez, M. A. Correa-Duarte, R. Dhama, G. Strangi, *ACS Photonics* **2014**, *1*, 371.
[33] M. El Kabbash, A. Rahimi Rashed, K. V. Sreekanth, A. De Luca, M. Infusino, G. Strangi, *J. Nanomater.* **2016**, *2016*, 1.
[34] A. Ferraro, D. C. Zografopoulos, M. A. Verschuuren, D. K. de Boer, F. Kong, H. P. Urbach, R. Beccherelli, R. Caputo, *ACS Appl. Mater. Interfaces* **2018**, *10*, 24750.
[35] H. Wei, D. Ratchford, X. Li, H. Xu, C.-K. Shih, *Nano Lett.* **2009**, *9*, 4168.
[36] V. E. Babicheva, N. Kinsey, G. V. Naik, M. Ferrera, A. V. Lavrinenko, V. M. Shalaev, A. Boltasseva, *Opt. Express* **2013**, *21*, 27326.
[37] G. V. Naik, V. M. Shalaev, A. Boltasseva, *Adv. Mater.* **2013**, *25*, 3264.
[38] C. Rhodes, S. Franzen, J.-P. Maria, M. Losego, D. N. Leonard, B. Laughlin, G. Duscher, S. Weibel, *J. Appl. Phys.* **2006**, *100*, 054905.
[39] Q. Bao, K. P. Loh, *ACS Nano* **2012**, *6*, 3677.
[40] G. R. Aizin, G. C. Dyer, *Phys. Rev. B* **2012**, *86*, 235316.
[41] Y. Luo, M. Chamanzar, A. Apuzzo, R. Salas-Montiel, K. N. Nguyen, S. Blaize, A. Adibi, *Nano Lett.* **2015**, *15*, 849.
[42] A. L. Pyayt, B. Wiley, Y. Xia, A. Chen, L. Dalton, *Nat. Nanotechnol.* **2008**, *3*, 660.
[43] A. A. Tseng, K. Chen, C. D. Chen, K. J. Ma, *IEEE Trans. Electron. Pack. Manuf.* **2003**, *26*, 141.
[44] E. A. Froning, K. A. Langner, *US Patent 4,983,197*, **1991**.
[45] R. F. Oulton, V. J. Sorger, D. Genov, D. Pile, X. Zhang, *Nat. Photonics* **2008**, *2*, 496.
[46] L. Vivien, S. Laval, B. Dumont, S. Lardenois, A. Koster, E. Cassan, *Opt. Commun.* **2002**, *210*, 43.
[47] D.-S. Song, S.-H. Kim, H.-G. Park, C.-K. Kim, Y.-H. Lee, *Appl. Phys. Lett.* **2002**, *80*, 3901.
[48] R. Salas-Montiel, M. Berthel, J. Beltran-Madrigal, S. Huant, A. Drezet, S. Blaize, *Nanotechnology* **2017**, *28*, 205207.
[49] K. L. Shlager, G. S. Smith, J. G. Maloney, *IEEE Trans. Antennas Propag.* **1994**, *42*, 975.
[50] G. Kewes, M. Schoengen, O. Neitzke, P. Lombardi, R.-S. Schönfeld, G. Mazzamuto, A. W. Schell, J. Probst, J. Wolters, B. Löchel, C. Toninelli, O. Benson, *Sci. Rep.* **2016**, *6*, 28877.

[51] W. Barnes, *J. Mod. Opt.* **1998**, *45*, 661.
[52] N. Kongsuwan, A. Demetriadou, R. Chikkaraddy, J. J. Baumberg, O. Hess, *EPJ Appl. Metamater.* **2018**, *5*, 6.
[53] D. Rocco, L. Carletti, A. Locatelli, C. De Angelis, *J. Opt. Soc. Am. B* **2017**, *34*, 1918.
[54] S. I. Bozhevolnyi, J. B. Khurgin, *Optica* **2016**, *3*, 1418.
[55] C. Ecoffet, A. Espanet, D. J. Lougnot, *Adv. Mater.* **1998**, *10*, 411.
[56] O. Soppera, S. Jradi, D. J. Lougnot, *J. Polym. Sci. A: Polym. Chem.* **2008**, *46*, 3783.
[57] G. E. Lio, J. B. Madrigal, X. Xu, Y. Peng, S. Pierini, C. Couteau, S. Jradi, R. Bachelot, R. Caputo, S. Blaize, *J. Phys. Chem. C* **2019**, *123*, 14669.
[58] R.-M. Ma, R. F. Oulton, V. J. Sorger, G. Bartal, X. Zhang, *Nat. Mater.* **2011**, *10*, 110.
[59] P. Kolchin, N. Pholchai, M. H. Mikkelsen, J. Oh, S. Ota, M. S. Islam, X. Yin, X. Zhang, *Nano Lett.* **2014**, *15*, 464.
[60] S. Dey, J. Zhao, *J. Phys. Chem. Lett.* **2016**, *7*, 2921.
[61] Y.-S. Lee, S.-D. Lin, *Opt. Express* **2014**, *22*, 1512.